Tethered Bilayer Lipid Membranes Based on Monolayers of Thiolipids Mixed with a Complementary Dilution Molecule. 1. Incorporation of Channel Peptides

ARTICLE *in* LANGMUIR · JANUARY 2006

Impact Factor: 4.46 · DOI: 10.1021/la051771p · Source: PubMed

7 AUTHORS, INCLUDING:

Lizhong He
Monash University (Australia)
60 PUBLICATIONS **919** CITATIONS
SEE PROFILE

Joseph W F Robertson
National Institute of Standards and Techno…
48 PUBLICATIONS **1,169** CITATIONS
SEE PROFILE

Stefan Schiller
University of Freiburg
43 PUBLICATIONS **1,199** CITATIONS
SEE PROFILE

Renate L. C. Naumann
AIT Austrian Institute of Technology
91 PUBLICATIONS **2,864** CITATIONS
SEE PROFILE

Tethered Bilayer Lipid Membranes Based on Monolayers of Thiolipids Mixed with a Complementary Dilution Molecule. 1. Incorporation of Channel Peptides

Lizhong He,† Joseph W. F. Robertson, Jing Li, Iris Kärcher, Stefan M. Schiller, Wolfgang Knoll, and Renate Naumann*

Max Planck Institute for Polymer Research, Ackermannweg 10, 55128 Mainz, Germany

Tethered bilayer lipid membranes (tBLMs) are described based on the self-assembly of a monolayer on template stripped gold of an archea analogue thiolipid, 2,3-di-*o*-phytanyl-sn-glycerol-1-tetraethylene glycol-D,L-α-lipoic acid ester lipid (DPTL), and a newly designed dilution molecule, tetraethylene glycol-D,L-α-lipoic acid ester (TEGL). The tBLM is completed by fusion of liposomes made from a mixture of diphytanoylphosphatidyl choline (DPhyPC), cholesterol, and 1,2-diphytanoyl-sn-glycero-3-phosphate (DPhyPG) in a molar ratio of 6:3:1. Melittin and gramicidin are incorporated into these tBLMs as shown by surface plasmon resonance (SPR) and electrochemical impedance spectroscopy (EIS) studies. Ionic conductivity at 0 V vs Ag|AgCl, 3 M KCl, measured by EIS measurements are comparable to the results obtained by other research groups. Admittance plots as a function of potential are discussed on a qualitative basis in terms of the kinetics of ion transport through the channels.

Introduction

Tethered bilayer lipid membranes (tBLMs) have been developed in the past decade as a model system of the biological membrane.[1−3] By engineering an ionically conductive submembrane compartment into a thiolipid monolayer, tBLMs provide a biomimetic platform for the investigation of membrane related proteins and processes such as ion transport across the lipid bilayer. tBLMs are generally prepared in a two-step procedure. The first step is the preparation of a self-assembled monolayer (SAM) of thiolipids[4−7] consisting of a lipid tail and a hydrophilic spacer attached to the metal substrate of gold or mercury via a mercapto-linker functionality. The tBLM is then completed in the second step by the fusion of liposomes prepared from phospholipids. A different strategy is to use a cocktail of thiolipids including transmembrane thiolipids, hydrophilic thiols, and phospholipids to form the complete tBLM in one step.[8−12] The role of the hydrophilic thiols used in the latter approach is to effectively dilute the tethering moiety on the surface. Previous attempts to dilute monolayers of thiolipids with short hydrophilic thiols, such as mercaptoethanol or lipoic acid, have generally resulted in bilayers with poor electrical properties (i.e., the nonspecific ionic conductivity is too high to observe ion channel behavior).[13]

Electrical properties of tBLMs are critically dependent on the chemical nature and composition of the self-assembling molecules.[4−23] Highly resistive tBLMs based on pure thiolipids with oxyethylene spacers have been obtained.[24−27] However, such tBLMs are only effective for the incorporation of small ion carriers such as valino-

* Corresponding author. E-mail: naumannr@mpip-mainz.mpg.de. Tel: ++49-6131-279 157.

† Present address: Centre for Nanostructure Bioengineering, Chemical Engineering Division, University of Queensland, St Lucia QLD 4072, Australia.

(1) Sinner, E.-K.; Knoll, W. *Curr. Opin. Chem. Biol*. **2001**, *5*, 705.
(2) Knoll, W.; Morigaki, K.; Naumann, R.; Saccà, B.; Schiller, St.; Sinner, E.-K. In *Ultrathin Electrochemical Chemo- and Biosensors, Technology and Performance*; Mirsky, V. M., Ed.; Springer: New York, 2004.
(3) Guidelli, R.; Aloisi, G.; Becucci, L.; Dolfi, A.; Moncelli, M. R.; Buoninsegni, F. T. *J. Electroanal. Chem.* **2001**, *504,* 1.
(4) Lang, H.; Duschl, C.; Vogel, H. *Langmuir* **1994**, *10*,197.
(5) Naumann, R.; Jonczyk, A.; Kopp, R.; Esch, J. v.; Ringsdorf, H.; Knoll, W.; Gräber, P. *Angew. Chem.* **1995**, *34*, 2056.
(6) Williams, L. M.; Evans, S. D.; Flynn, T. M.; Marsh, A.; Knowles, P. F.; Bushby, R. J.; Boden, N. *Langmuir* **1997**, *13*, 751.
(7) Bunjes, N.; Schmidt, E. K.; Jonczyk, A.; Rippmann, F.; Beyer, D.; Ringsdorf, H.; Gräber, P.; Knoll, W.; Naumann, R. *Langmuir* **1997**, *13*, 6188.
(8) Cornell, B. A.; Braach-Maksvytis, V. L. B.; King, L. G.; Osman, P. D.; Raguse, J.; Wieczorek, L.; Pace, R. J. *Nature* **1997**, *387*, 580.
(9) Raguse, B.; Braach-Maksvytis, V.; Cornell, B.; A.; King, L. G.; Osman, P. D. J.; Pace, R. J.; Wiezcorek, L. *Langmuir* **1998**, *14*, 648.
(10) Woodhouse, G.; E.; King, L. G.; Wiezcorek, L.; Cornell, B. A. *Faraday Disc.* **1998**, *111*, 247.
(11) Cornell, B. A.; Krishna, G.; Osman, P. D.; Pace, R. J.; Wieczorek, L. *Biochem. Soc. Trans.* **2001**, *29*, 613.
(12) Krishna, G.; Schulte, J.; Cornell, B. A.; Pace, R.; Wieczorek, L.; Osman, P. D. *Langmuir* **2001**, *17*, 4858.
(13) Baumgart, T.; Kreiter, M.; Lauer, H.; Naumann, R.; Jung, G.; Jonczyk, A.; Offenhäusser, A.; Knoll, W. *J. Colloid Interface Sci.* **2003**, *258*, 298.
(14) Vanderah, D. J.; Meuse, C. W.; Silin, V.; Plant, A. L. *Langmuir* **1998**, *14*, 6916.
(15) Krueger, S.; Meuse, C. W.; Majkrzak, C. F.; Dura, J. A.; Berk, N. F.; Tarek, M.; Plant, A. L. *Langmuir* **2001**, *17,* 511.
(16) Schmidt, E. K.; Liebermann, T.; Kreiter, M.; Jonczyk, A.; Naumann, R.; Offenhäusser, A.; Neumann, E.; Kukol, A.; Maelicke, A.; Knoll, W. *Biosens. Bioelectron.* **1998**, *13,* 585.
(17) Naumann, R.; Schmidt, E. K.; Jonczyk, A.; Fendler, K.; Kadenbach, B.; Liebermann, T.; Offenhäusser, A.; Knoll, W. *Biosens. Bioelectron.* **1999**, *14,* 651.
(18) Naumann, R.; Baumgart, T.; Gräber, P.; Jonczyk, A.; Offenhäusser, A.; Knoll, W. *Biosens. Bioelectron.* **2002**, *17*, 25.
(19) Glazier, S. A.; Vanderah, D. J.; Plant, A. L.; Bayley, H.; Valincius, G.; Kasianovic, J. *Langmuir* **2000**, *16*, 10428.
(20) Madhusudhana, N.; Silin, V.; Ridge, K. D.; Woodward, J. T.; Plant, A. L. *Anal. Biochem.* **2002**, *307*, 117.
(21) Peggion, C.; Formaggio, F.; Toniolo, C.; Becucci, L.; Moncelli, M. R.; Guidelli, R. *Langmuir* **2001**, *17*, 6585.
(22) Krysinsky, P.; Zebrowska, A.; Michota, A.; Bukowska, J.; Becucci, L.; Moncelli, M. R. *Langmuir* **2001**, *17*, 3852.
(23) Becucci, L.; Guidelli, R.; Liu, Q.; Bushby, R. J.; Evans, S. D. *J. Phys. Chem. B* **2002**, *106,* 10410.
(24) Schiller, S. M.; Naumann, R.; Lovejoy, K.; Kunz, H.; Knoll, W. *Angew. Chem., Int. Ed*. **2003**, *42*, 208.
(25) Naumann, R.; Schiller, S. M.; Giess, F.; Grohe, B.; Hartman, K. B.; Kärcher, I.; Köper, I.; Lübben, J.; Vasilev, K.; Knoll, W. *Langmuir* **2003**, *19*, 5435.
(26) Moncelli, M. R.; Becucci, L.; Schiller, S. M. *Biolectrochemistry* **2004**, *63*, 161.
(27) Terretaz, S.; Mayer, M.; Vogel, H. *Langmuir* **2003**, *19*, 5567.

mycin.[28] Larger peptides typically adsorb to the surface of these tBLMs if gold surfaces are used as the support.[29] This is different on mercury, where, due to the enhanced fluidity of the metal, larger ion channels have been successfully incorporated into bilayers based on monolayers of thiolipids.[26]

For Au substrates, the tethering molecule in the SAM must be spatially diluted to allow for larger peptides to be incorporated into a bilayer.[8−12] tBLMs based on thiol-modified ion channels have been reported as an alternative.[27] Here we report on a newly designed hydrophilic thiol provided with a tetraethylene glycol moiety to prepare mixed monolayers on gold with the previously described archea analogue thiolipid.[24,25] Dilution molecules bearing short chain ethoxy groups were found to promote the formation of lipid bilayers in an otherwise completely different approach.[30] This finding is in agreement with our results regarding the above-mentioned mixed monolayers. Highly insulating tBLMs are obtained by fusion with liposomes into which single helical ion channels, such as melittin and gramicidin, are shown to incorporate. Ion transport through the channels is followed by electrochemical impedance spectroscopy (EIS).

By utilizing the two-step procedure described previously[24,25] and herein for the formation of tBLMs, real-time analysis by SPR and stepwise analysis by EIS analysis can be performed to optimize the formation of these tBLMs. The additional level of control afforded by the real-time analysis allows for delicate control of the timing for vesicle fusion in order to fabricate complete bilayers while avoiding vesicle adsorption.

Experimental Section

Diphytanoylphosphatidyl choline (DPhyPC), 1,2-diphytanoyl-sn-glycero-3-phosphate (DPhyPG), and cholesterol were supplied from Avanti Polar Lipids, Inc., Alabaster, Al, USA; sodium chloride (SigmaUltra), potassium chloride, *N*-(2-hydroxyethyl)-piperazine-*N*′-(2-ethanesulfonic acid) HEPES, and gramicidin D from *bacillus brevis* were obtained from Sigma-Aldrich; melittin was supplied from Fluka, Buchs, Switzerland. Purified water (>18 MΩ cm) from a Milli-Q (Millipore, Inc) system was used throughout.

The synthesis of the thiolipid 2,3-di-*O*-phytanyl-sn-glycerol-1-tetraethylene glycol-D,L-α-lipoic acid ester lipid (DPTL) was carried out as previously described.[24] For the synthesis of the dilution molecule tetraethylene glycol-D,L-α-lipoic acid ester (TEGL), D,L-α-lipoic acid (5.0 g, 24.2 mmol) was dissolved in 75 mL of dry methylene chlorid. Dicyclohexyl carbodiimide (5.0 g, 24.2 mol), dissolved in 75 mL of dry methylene chloride was added and the solution stirred at room temperature for 15 min under argon. Tetraethylene glycol (14.12 g, 72.7 mmol) was dissolved in 75 mL of dry methylene chloride and deprotonated with sodium hydride (0.87 g, 0.0364 mol) and stirred for 15 min. The solutions were combined, and 4-(dimethylamino)pyridine (DMAP, 30 mg, 0.245 mmol) was added and the reaction mixture and stirred for 48 h under argon at room temperature. The solvent was removed under reduced pressure and the crude product purified on silica gel with ethyl acetate, yielding 2.56 g (28%) of the desired tetraethylene glycol-D,L-α-lipoic acid ester as a slightly yellow oil. $R_f = 0.36$ (ethyl acetate). *m/z* (Maldi-TOF MS) = 382 (M^+, 100%); $C_{16}H_{30}O_6S_2$ (382,54) calculated: C, 50.24; H, 7.90; O, 25.09; S, 16.76; found: C, 50.19; H, 7.92; O, 25.17; S, 16.57. ^{1}HNMR ($CDCl_3$) δ 4.21−4.25 (2H, m, (−(O=C)−O−CH_2−CH_2−O−)), 3.53−3.74 (14H, m, (−CH_2−CH_2−O−)), 3.59−3.61 (1H, m, (S−S−CH−)), 3.05−3.22 (2H, m, (−CH_2−CH_2−S−S−)), 2.32−2.52 (1H, m, (−CH_2−CH_2−S−S−)), 2.32−2.38 (2H, m, (−CH_2−CH_2−(O=C)−)), 1.84−1.96 (1H, m, (−CH_2−CH_2−S−S−)), 1.60−1.74 (4H, m, (−CH_2−CH_2−(O=C)−) & (−S−CH−(CH_2−CH_2−S−)−CH_2−), 1.41−1.52 (2H, m, (−CH_2−CH_2−CH_2−(O=C)−); ^{13}CNMR ($CDCl_3$) δ 173.25 (*C*=O), 72.39 (−*C*H_2−CH_2−OH), 70.46 (−CH_2−*C*H_2−O−CH_2−), 70.36 (−CH_2-*C*H_2−O−CH_2-), 70.15 (−CH_2−*C*H_2−O−CH_2−), 69.00 (−(O=C)−O−CH_2−*C*H_2−O−), 63.25 (−(O=C)−O−*C*H_2−CH_2−O−), 61.52 (−CH_2−*C*H_2−OH), 56.10 (S−S−*C*H−), 40.47 (−*C*H_2−CH_2−S−S−), 38.31 (−CH_2−*C*H_2−S−S−), 34.41 (−S−CH−(CH_2−CH_2−S−)−*C*H_2−), 33.75 (−CH_2−*C*H_2−(O=C)−), 28.53 (−*C*H_2−CH_2−CH_2−(O=C)−), 24.43 (−*C*H_2−CH_2−(O=C)−).

TEGL is soluble in methanol, ethanol, and trifluorethanol but has a tendency to oxidize after which it dissolves only after prolonged stirring of the suspension. Only monomers are found in the solution with no indication of higher oligo- or polymers.

Preparation of the Template Stripped Gold (TSG) Surface. Gold films (50 nm thick) were deposited by electrothermal evaporation (rate 0.01−0.05 nm/s, 2×10^{-6} mbar) on silicon wafers. Gold films on silicon wafers were then glued with EPO-TEK 353ND-4, ($n = 1.5922$ at 633 nm) to LaSFN9 glass slides and cured for 60 min at 150°C. The silicon wafers were detached from the gold film immediately before use. Characterization of these Au films can be found in ref 25.

Preparation of the Liposomes. DPhyPC, cholesterol, and DPhyPG were dissolved in chloroform at a molar ratio of 6:3:1. The solvent was evaporated and the residue was hydrated at 40 °C in Milli-Q water at a concentration of 1 mg lipid/mL for 4 h. Thereafter liposomes were prepared by extrusion through a 50 nm polycarbonate filter. The solution was then diluted with water to a final concentration 0.2 mg/mL.

Surface Preparation. TSG slides were placed for 24 h in a mixed solution DPTL/TEGL (0.2/0.02 mM) in ethanol rinsed in pure ethanol and dried in a stream of nitrogen.

For melittin-containing bilayers, the SAMs were placed in a buffer solution of NaCl (140 mM), KCl (6 mM), and HEPES (10 mM) pH 7.4 and mixed liposomes were added for a final lipid concentration of 0.04 mg/mL. Vesicle fusion was monitored by SPR, and shortly before the kinetic trace reached saturation, 20 μL of a melittin stock solution (0.65 mg/mL in ethanol $\equiv 2.28 \times 10^{-4}$ M) was added to 1 mL of the bathing solution to obtain a final concentration of 4.57×10^{-6} M.

For gramicidin D containing bilayers, SAMs were placed in a buffer solution of KCl (50 mM) and HEPES (10 mM) pH 7.4 and mixed liposomes were added for a final concentration 0.04 mg/mL. Vesicle fusion was monitored by SPR, and shortly before the kinetic trace reached saturation, gramicidin D was added to a final concentration of 4×10^{-7} M in the bathing solution, from a stock solution (8×10^{-5} M) in ethanol.

Analytical Methodologies. *Surface Plasmon Spectroscopy.* SPR was performed in a setup as described previously using the Kretschmann configuration.[31] The glass slide (LaSFN9 glass from Hellma Optik, Jena, refractive index $n = 1.85$ at 633 nm) was optically matched to the base of a 90° glass prism (LaSFN9). Monochromatic light from a He/Ne laser (Uniphase, San Jose, CA, $\lambda = 632.8$ nm) was directed through the prism and collected by a custom-made photodiode detector. Based on a fitting routine using the Fresnel equations, the following parameters of the planar multilayer system were evaluated as given in Table 1 with ϵ and d being the dielectric constant and the thickness of the layers, respectively. The parameters d_{gold}, ϵ_{gold}, and ϵ_{water} were obtained by a reference scan taken from a clean gold surface of

Table 1. Optical Constants (d = Thickness, ϵ = Dielectric Constant) Used for SPR Fitting

layer	d/nm	ϵ
glass	←	3.14[a]
gold	∼50[b]	−12.1 + i*1.2[a]
thiolipid	fitted	2.10[a]
phospholipid	fitted	2.25[a]
water (buffer)	←	1.77[a]

[a] Obtained from independent sources.[31] [b] Calculated from a reference sample.

(28) Naumann, R.; Walz, D.; Schiller, S. M.; Knoll, W. *J. Electroanal. Chem.* **2003**, *550−551*, 241.

(29) Vitovic, P.; Kresak, S.; Naumann, R.; Schiller, S. M.; Lewis, R. N. A. H.; McElHaney, R. N.; Hianik, T. *Bioelectrochemistry* **2004**, *63*, 169.

(30) Eli-Caille, C.; Fliniaux, O.; Pantigny, J.; Mazière, J.-C.; Bourdillon, C. *Langmuir* **2005**, in press.

(31) Knoll, W. *Annu. Rev. Phys. Chem.* **1998**, *49*, 569.

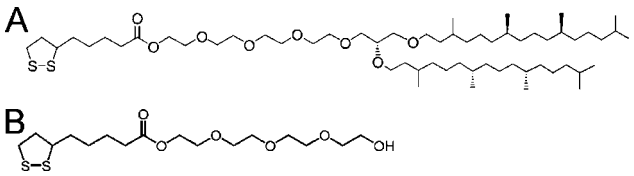

Figure 1. Molecules used for the formation of the mixed monolayers. (A) 2,3-Di-O-phytanyl-sn-glycerol-1-tetraethylene glycol-D,L-α-lipoic acid ester (DPTL), (B) tetraethylene glycol-D,L-α-lipoic acid ester (TEGL).

the same thickness. $\epsilon_{\text{thiolipid}}$ is a reasonable assumption from $\epsilon_{\text{phospholipid}}$, which is assumed to be equivalent to a pure alkane. Fusion of liposomes with the mixed SAMs was followed by recording the reflectivity as a function of time for a fixed angle, $\theta = 56.5°$. The recording was transferred into a time-dependent increase of the thickness by calibration of the start- and endpoint. For small shifts in the resonance angle, the intensity in the quasi-linear range of the reflectivity scan can be assumed to be a linear function of the layer thickness.

Electrochemistry. EIS experiments were performed with an EG&G 273 potentiostat/galvanostat equipped with a Solartron 1260 frequency response analyzer. Potential control and data collection were obtained with the Zplot/Zview software package (Scribner Associates, Inc). A three-electrode setup was employed using a Pt wire counter electrode and a reference electrode Ag|AgCl, 3 M KCl. Experiments were performed in the buffer solutions described above for the different channel peptides.

Data analysis was performed by utilizing the equivalent circuit-fitting algorithm included in Zview. Data are fitted using the simplest model that adequately describes the data. To account for a distribution of time constants a constant phase element (CPE) was used. The CPE has the general form

$$Z_{\text{CPE}} = (A_{\text{CPE}} j\omega)^{-\alpha} \tag{1}$$

where Z_{CPE} is the frequency dependent impedance of the CPE, A_{CPE} is the software determined fit value with units $(\text{F cm}^{-2})^{\alpha}$, ω is the frequency in rad/s and α represents the deviation from a pure capacitor (when $\alpha = 1$, A_{CPE} becomes a capacitance).

Melittin experiments utilized an electrolyte solution of 140 nM NaCl, 6 mM KCl, and 10 mM HEPES buffered to a pH of 7.4. Three different electrolyte solutions were used for gramicidin: buffer A (50 mM KCl and 10 mM HEPES buffered to pH 7.4), buffer B (100 mM NaCl and 10 mM HEPES buffered to pH 7.4), and buffer C (10 mM Imidazol and 50 mM tetramethylammonium chloride buffered to pH 7.4).

Atomic Force Microscopy. AFM images were acquired with a Nanoscope IIIa scanning probe microscope (Digital Instruments, Santa Barbara, CA). Images were collected in TappingMode with Olympus OMCL-AC160TS−W2 Non-Contact/TappingMode tips.

Contact Angle Measurements. Contact angle measurements were acquired on a Kruess model-DSA10 Drop shape analysis system. A 2 μL drop of water was placed on a surface from a syringe needle. The drop image was then captured with a video camera modified with a microscope and then saved to a computer. The method used to calculate the contact angle from the drop image is termed Tangent Method 1 (Kruess model DSA10 User Manual).

Results and Discussion

Mixed-monolayers were prepared from solutions of DPTL mixed with TEGL in ethanol, and Figure 1 displays the structure of both molecules which are identical regarding the tetraethyleneglycol lipoic acid ester moiety. The dilution molecule is small compared to the thiolipid and hence might experience kinetic advantage toward chemisorption on the gold surface so that the mixing ratio on the surface would be different from the one in solution 10/90 (TEGL/DPTL). Reductive desorption experiments were performed, although peak separation was insufficient to determine the relative proportion of thiols assembled on the surface. From the water contact angle of the mixed monolayer, however, the mixing ratio can be calculated according to an investigation carried out on monolayers of cholesterol functionalized thiol derivatives mixed with mercaptoethanol. [32] These authors showed a linear dependency between the percentage of cholesterol lipid and the cosine of the contact angle according to Cassie's law

$$\cos\theta = f_1 \cos\theta_1 + f_2 \cos\theta_2 \tag{2}$$

where θ, θ_1, and θ_2 are the advancing contact angles on the mixed surface and the two single component surfaces, respectively, and f_1 and f_2 are the fractions of each component present in the mixed monolayer.[33] The contact angle of the mixed monolayer in the present case was $\theta = 95°$, compared to $\theta = 109°$ of a pure DPTL monolayer[25] and $\theta = 25°$ of a pure TEGL monolayer. The mixing ratio on the surface calculated from these values was 20/80 (TEGL/DPTL).

The mixed monolayers are not expected to show significant aggregation because of the relatively low van der Waals interactions present between the bulky phytanoyl chains. Mixed monolayers were first investigated by AFM in an attempt to prove the absence of lateral segregation of the two molecules. Figure 2 shows the comparison of an unmodified TSG surface (Figure 2A) and a TSG surface modified with a mixed monolayer of DPTL/TEGL (Figure 2B). Figure 2A show a typical TSG surface with some slight inhomogeneity of the Au grain structure across the 1 μm^2 surface area of this analysis. The root-mean-square (RMS) roughness for this surface is 0.29 nm with a maximum peak-to-valley height of <2 nm. If a mixed monolayer is adsorbed on the surface, the RMS roughness increases to 0.30 nm with a similar peak-to-valley roughness. The components of the mixed SAM, DPTL, and TEGL seem to be evenly distributed giving rise to very smooth surfaces with no significant increase of the roughness with respect to pure TSG.[25,33] However, the AFM procedure more appropriate to detect phase separation is lateral force microscopy. The result is shown in Figure 2c also giving no indication of an appreciable segregation.

As far as vesicle fusion on these mixed monolayers is concerned, hydrophobic interaction should provide a significant driving force, considering the water contact angle mentioned above.[34,35] Lipid composition of the vesicles also shows an influence on the fusion process. Composition and molecular shape of the lipids determine the physical properties of the lipid membrane (e.g., membrane fluidity, bilayer thickness, surface charge distribution, and lateral pressure). Consequently, these properties affect the structure and function of incorporated ion channels.[36] For example, cholesterol can influence the function of membrane proteins both by binding directly to the proteins and by changing biophysical properties of the lipid membrane. Cholesterol has thus been used with planar supported lipids to give the bilayer more cohesion on a planar surface.[37] One distinct aspect of the present work is that we employ liposomes from a mixture of a charged diphytanoyl lipid (DPhyPG), a neutral di-

(32) Williams, L. M.; Evans, St. D.; Flynn, Th. M.; Marsh, A.; Knowles, P. F.; Bushby, R. R. J.; Boden, N. J. *Langmuir* **1997**, *13*, 751.
(33) Kalb, E.; Frey, S.; Tamm, L. K. *Biochim. Biophys. Acta*, **1992**, *1103*, 307.
(34) Wagner, P.; Hegner, M.; Güntherodt, H.-J.; Semenza, G. *Langmuir* **1995**, *11*, 3967.
(35) Keller, C. A.; Kasemo, B. *Biophys. J.* **1998**, *75*, 1397.
(36) Keller, C. A.; Glasmästar, K.; Zhdanov, V. P.; Kasemo, B. *Phys. Rev. Lett.* **2000**, *84*, 5443.
(37) Tillman, T. S.; Cascio, M. *Cell Biochem. Biophys*. **2003**, *38*, 161.

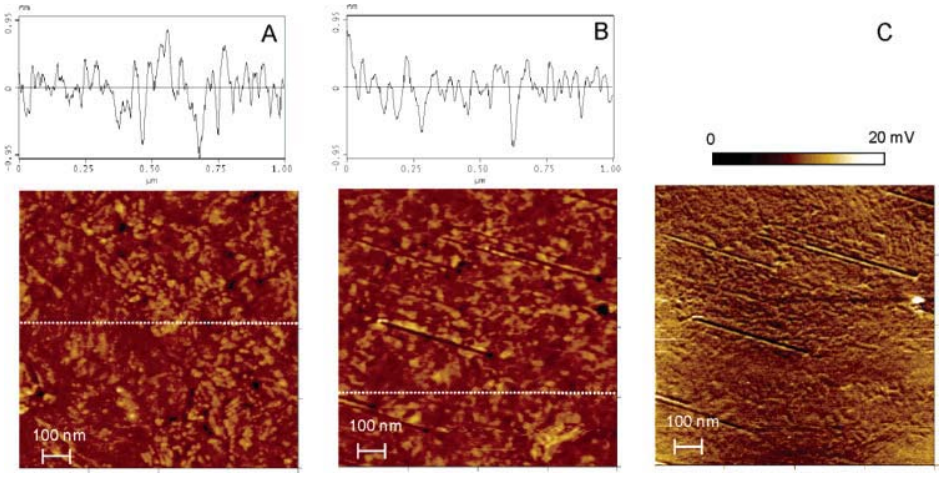

Figure 2. Contact mode AFM images of template stripped gold (TSG) before (A) and after (B) formation of the mixed SAM of DPTL/TEGL. The surface roughness of each sample is given at the top of (A) and (B). Curve (C) represents the friction mode AFM image of the mixed SAM.

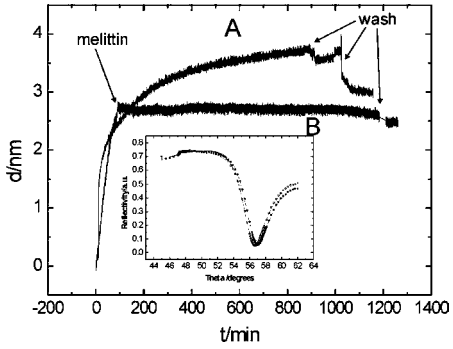

Figure 3. Thickness as a function of time at a fixed angle of incidence of the surface plasmon resonance spectrum during vesicle fusion on a DPTL/TEGL mixed SAM in a buffer solution NaCl (140 mM/L), KCl (6 mM/L), and HEPES (10 mM/L) pH 7.4. (A) Kinetics of thickness increase after adding SUVs made from DPhyPC, cholesterol and DPhyPG and (B) when adding a solution of melittin to a final concentration of 4.57 μM from a stock solution 228 μM, shortly before the curve goes into saturation. Thicknesses obtained from reflectivity scans shown in the inset are used for the calibration.

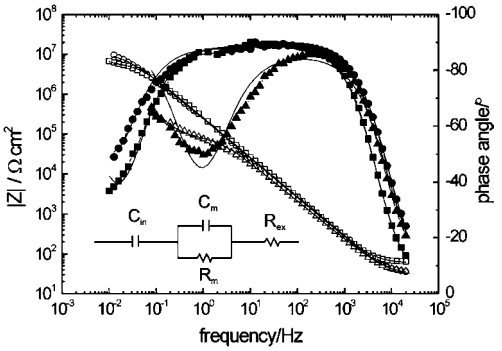

Figure 4. Electrochemical impedance spectra of the mixed SAM in a buffer solution NaCl (140 mM), KCl (6 mM), and HEPES (10 mM) pH 7.4, before (□, ■) and after fusion with liposomes without (○, ●) and with (△, ▲) melittin to a final concentration of 4.57 μM. All measurements were conducted at a bias potential of 0 V vs Ag/AgCl. Continuous curves are data fitted to the equivalent circuit given in the inset where C_m is represented by a CPE and α is the distribution factor. For the explanation of the other parameters, see the text. Parameters from the fits are included in Table 2.

phytanoyl lipid (DPhyPC), and cholesterol. Such a mixture of different lipids seems crucial to achieve good resistivity to nonspecific ion transport across the supported lipid membrane. Furthermore, by using liposomes prepared in pure water, additional osmotic shock was utilized to promote the fusion process since a relatively high ionic strength electrolyte was used for the bathing solution.

Figure 3A shows the resulting SPR kinetic trace, which is the reflectivity at a fixed angle of incidence vs time. In these data, the thickness increased rapidly for the first ~30 min and then continued to gradually increase well beyond the 2.5 nm expected for the second bilayer leaflet. The continuous gradual increase of the thickness in the kinetic trace is indicative of adsorption of additional liposomes. Some of the adsorbed liposomes can be washed off the surface when the surface is rinsed with the original buffer solution. When melittin is injected during the early stages of fusion (~60 min, Figure 3B), a plateau in thickness of ~2.7 nm is abruptly reached. Thus, melittin appears to aid in the stability of the bilayer structure.

Electrochemical Characterization. Mixed SAMs before and after vesicle fusion were further investigated by electrochemical impedance spectroscopy (EIS). Figure 4 shows Bode plots of the spectra before (□, ■) and after (○, ●) completion of the fusion process. Spectra were fitted to the equivalent circuit shown in the inset of Figure 4, which consists of a solution resistance R_{ex} in series with the membrane resistance and capacitance, R_m and C_m respectively, in series with an internal reservoir capacitance, C_{in}. Capacitance and resistance of the monolayer was in the range of 0.8−1.2 μF cm^{-2} and 1−2 MΩ cm^2, respectively, according to the high proportion of the thiolipid. A constant phase element (CPE) was introduced into the equivalent circuit in place of C_m to account for the heterogeneity of the mixed layers. During fusion, the resistance increased from 5 to 10 MΩ cm^2 and the capacitance decreased from 0.88 to 0.73 μF cm^{-2} due to the increased thickness of the alkyl moiety from the lipid

Table 2. EIS Fitting Parameters for the Data in Figure 5[a]

surface	R_m/ MΩ cm^2	A_{CPE}/ (F cm^{-2})$^\alpha$	α	C_{in}/ μF cm^{-2}
SAM	5.1	0.88	0.98	3.2
lipid bilayer	7.4	0.73	0.99	5.0
lipid bilayer with melittin	0.062	1.1	0.95	4.8

[a] A_{CPE} is the fit parameter for the CPE obtained from the ZVIEW fit routine, and α represents the distribution parameter of time constants. For α = 1, the CPE becomes a pure capacitor.

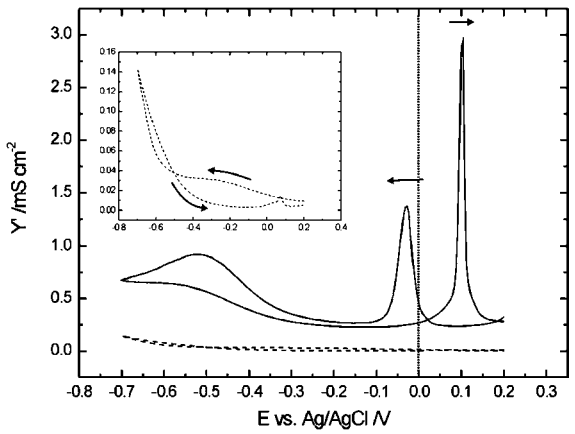

Figure 5. In phase component of the admittance as a function of potential at a scan rate of 10 mV/s and a fixed frequency of 10 Hz of the mixed tBLM in a buffer solution NaCl (140 mM), KCl (6 mM), and HEPES (10 mM) pH 7.4, with (—) and without (- - -) melittin incorporated to a final concentration of 4.57 μM. The inset shows an enlarged plot of the blank curve without mellitin.

bilayer. If an ethanolic solution of melittin was added toward the final stage of vesicle fusion, the resistance decreased from 7.4 MΩ cm^2 to 60 kΩ cm^2 indicating ionic conductivity through the melittin channel. Throughout the experiment, the inner membrane capacitance remained relatively unchanged.

Although EIS results show a clear transport of K^+ ions across the membrane, more detailed information can be extracted from the membrane/protein superstructure by monitoring the conductivity as a function of applied potential as measured by the in-phase component, $Y\Re$of the electrode admittance at 10 Hz. In this case a potential sweep of ~10 mV/s was used with a 10 mV AC perturbation between +0.2 and −0.7 V. The results are shown in Figure 5.

Initially, the conductivity of a tBLM prepared without any channel-forming protein was examined. A steady increase in the conductivity from +0.2 to ~−0.6 V was observed which indicates a slight decrease in the insulating properties of the bilayer. At −0.6 V the conductivity increased rapidly, indicating significant failure in the stability of the tBLM. The reverse cycle showed a rapid decrease in the conductance until ~−0.4 V (see inset) where the conductivity reduces to $<1 \times 10^{-6}$ S/cm^2. In the reverse sweep, a small peak was observed likely suggesting either expulsion of any residual cations within the submembrane space or a rearrangement of the tBLM. Despite the clear features in the plot, the insulating properties of the tBLM are clearly good enough to discriminate between specific ion transport through a protein and the simple electric-field driven ion transport through the membrane. Additionally, at large negative potentials, the membrane stability decreases, presumably allowing for additional cations to access the submembrane space. Nevertheless, the decrease in stability is fully reversible as the potential is swept in the reverse direction. It should be noted that the exact potentials for membrane breakdown and cation transient peaks are highly dependent on the quality (insulation) of the membrane itself.

If melittin is incorporated into the bilayer and 6 mM K^+ are present in the solution, a conductance is noted at ~2.5 $\times$ 10^{-4} S/cm^2, which is significantly higher than the respective value of the channel free tBLM. As the potential is scanned from positive to negative potentials, a sharp peak at ~−0.032 V (fwhm ≈ 33 mV) ~1.4 $\times$ 10^{-3} S/cm^2 in height is observed, followed by a steady-state conductance of 2.7 $\times$ 10^{-4} S/cm^2. Beyond ~−0.3 V, the conductance increases until a broad peak is reached at −0.52 V. In the reverse scan, the conductivity decays gradually from −0.7 to ~−0.3 V, where a similar steady state is reached. After that, the reverse scan maintains a conductivity of 2.3 $\times$ 10^{-4} S/cm^2 until a narrow peak (fwhm ≈ 12 mV) at +0.101 V is observed. Beyond the peak the conductivity attains the original basic conductance of ~2.5 $\times$ 10^{-4} S/cm^2.

Melittin is a polypeptide that binds to biomembranes such as BLMs where, at low concentrations, it induces voltage-gated channels.[38] When bound to lipid bilayers, it adopts a α-helical conformation with most hydrophobic residues located on one side and most hydrophilic residues located on the opposite side of the helix long axis. At zero voltage, these amphipathic helices are believed to accumulate on the surface of the membrane parallel to the plane of the bilayer. At voltages negative on the opposite side with respect to the melittin, the helices form membrane spanning aggregates that induce pore conductance.[39] Melittin has been incorporated into tBLMs also on Hg and analyzed by impedance spectroscopy.[26,39] A similar peak shaped signal was obtained in the admittance plot in the case of tBLMs based on the same DPTL molecule used in the present investigation, [26] whereas in tBLMs based on oligoethyleneoxythiols a sigmoidic increase of the conductivity was obtained. [23] However, in both cases, the potentials at which the signals were observed were shifted in the negative direction as compared to the gold surface. This is not surprising in view of the differences in the potential of zero charge (pzc) of both metals. Actually, Guidelli et al. made use the admittance plots of valinomycin inserted into a tBLM on mercury and on gold to find out about the potential difference across the stratified layer and as a proof of principle of eq 3 [40]

$$\Delta\phi - \chi_e \equiv \psi = \sigma_M(C_{OEO}{}^{-1} + C_{mem}{}^{-1}) + \chi_{OEO} + \chi_{PC,PG} \quad (3)$$

where $\Delta\phi - \chi_e$ is the applied potential, $\Delta\phi$, corrected for the dipole potential at the metal interface, χ_e, resulting in ψ, the potential difference across the entire gold|solution interface, σ_M is the surface charge density on the Au electrode, C_{OEO} and C_{mem} are the capacitances of the submembrane space and the membrane, respectively, and χ_{OEO} is the permanent dipole potential of the OEO groups in the submembrane space and $\chi_{PC,PG}$ in the dipole potential of the phospholipid. According to this equation, the potential drop across the interface is determined by the relative capacitances of each effective layer of the monolayer/bilayer system. If we assume that the dipole moments for the spacer and lipid do not change with potential, we can show that 90−95% of the overall effective potential, ψ, drops across the lipid membrane, whereas only 5−10% drops across the OEO spacer. This arises naturally from the relative capacitance of each "layer" previously determined from EIS measurements. Moreover, from this equation, the overall potential, ψ, can be obtained at which the transmembrane potential vanishes. This effective potential is not known due to the uncertainty in the dipole potential at the metal interface,

(38) Purrucker, O.; Hillebrandt, H.; Adlkofer, K.; Tanaka, M. *Electrochim. Acta* **2001**, *47*, 791.
(39) Pawlak, M.; Stankowski, S.; Schwarz, G. *Biochim. Biophys. Acta* **1991**, *1062*, 94.
(40) Becucci, L.; Moncelli, M. R.; Guidelli, R *Langmuir* **2003**, *19*, 3386.

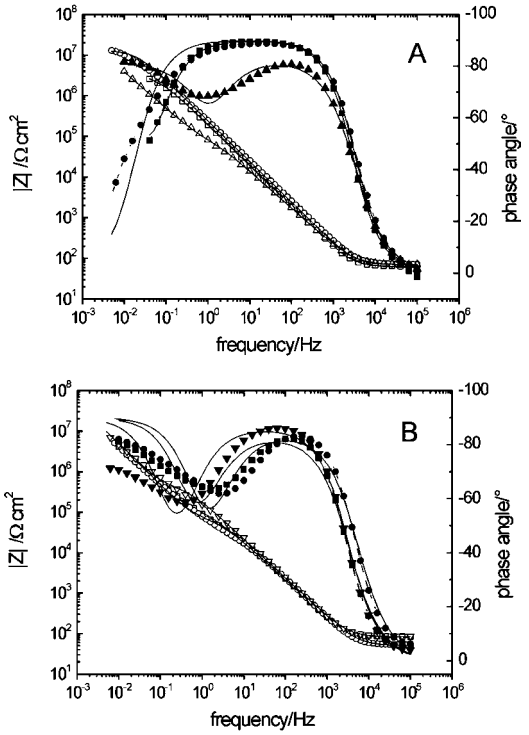

Figure 6. (A) Electrochemical impedance spectra of the mixed SAM in a buffer solution KCl (50 mM) and HEPES (10 mM) pH 7.4 (buffer A) before (□, ■) and after fusion with liposomes without (○, ●) and with (△, ▲) gramicidin D added (final concentration of 0.4 μM in the bathing solution). (B) With gramicidin added in buffer A (50 mM K^+ □, ■), B (100 mM Na^+ ○, ●), and C (50 mM $(CH_3)_4N^+$ △, ▲). All measurements were conducted at a bias potential of 0 V vs Ag|AgCl. Continuous curves are data fitted to the equivalent circuit given in the inset of Figure 4, parameters from the fits are included in Table 3.

χ_e, of the polycrystalline gold surface due to electron spillover. However, comparative measurements of valinomycin doped tBLMs on gold and on mercury performed by the Guidelli group indicated a shift in the positive direction on the gold surface. The applied potential vs SCE when the potential across the bilayer vanishes on gold was expected to lie at about +0.200 V,[40] whereas the pzc of polycrystalline gold was reported to be +0.003 V vs Ag|AgCl, 3M KCl.[41] In any case, at potentials at positive extremes, K^+ ions should be driven out of the submembrane space to equilibrate the potential gradient/concentration difference existing across the membrane whereas at negative extremes they are driven in. From this consideration applied to the result shown in Figure 5 as well as Figure 7 further below, the applied potential at which the transmembrane potential vanishes would be deduced to lie at around +0.05 V vs Ag|AgCl in our case.

Similar observations were made on the mixed tBLM with gramicidin incorporated. The impedance spectra of the monolayer and bilayer with and without gramicidin are shown in Figure 6A. An increase of the resistance and decrease of the capacitance due to bilayer formation is observed as demonstrated in Figure 5 as well as Figure 6A. In this case, the capacitance decreases from 1.1 to 0.74 μF/cm^2 while the resistance increases from 2.1 to 8.7 MΩ cm^2, which when taken together indicates a tight

(41) Trasatti, S.; Lust, E. In *Modern Aspects of Electrochemistry*; White, R. E., Bockris, J. O'M., Conway, B. E., Eds.; Kluwer/Plenum: New York, 1999; Vol. 33, p 1.

Table 3. EIS Fitting Parameters for the Data in Figure 7

surface/buffer	R_m/ MΩ cm^2	C_m/ μF cm^{-2}	C_{in}/ μF cm^{-2}
SAM[a]	2.1	1.1	3.4
lipid bilayer[a]	8.7	0.74	5.1
lipid bilayer with gramicidin			
buffer A	0.036	0.98	3.3
buffer B	0.053	0.99	3.2
buffer C	0.25	0.88	3.0

[a] Measurements performed in a buffer solution KCl (50 mM) and HEPES (10 mM) pH 7.4 (buffer A).

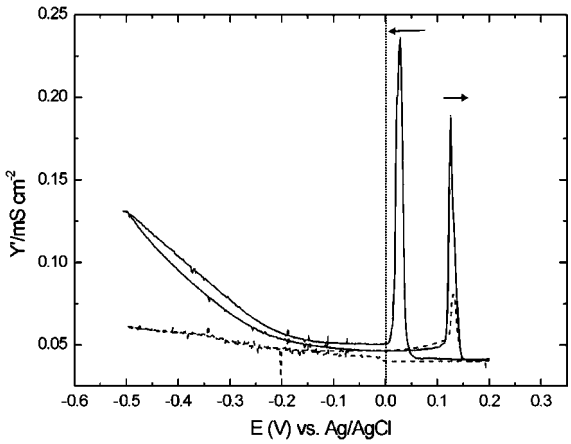

Figure 7. In phase component of the admittance as a function of potential at a scan rate of 10 mV/s and a fixed frequency of 10 Hz of the mixed tBLM with gramicidin D incorporated (final concentration of 4×10^{-7} M in the bathing solution), (—) Buffer A [KCl (50 mM), HEPES (10 mM) pH 7.4]; (- - -)Buffer C [imidazol (10 mM) tetramethylammonium chloride (50 mM) pH 7.4].

bilayer. If gramicidin is incorporated, the resistance of the membrane drops to 36 kΩ cm^2 corresponding to 27 μS cm^{-2}. These values are in agreement with the 29 kΩ cm^2 reported by Purrucker et al. for K^+ conductivity through the gramicidin D channel inserted into a lipid bilayer prepared from a lipid mixture containing cholesterol on a Si/SiO_2 surface.[38] Figure 6B shows the result if the cation in the bathing solution is changed from 50 mM K^+ (buffer A, □, ■) to 100 mM Na^+ (buffer B, ○, ●) to 50 mM $(CH_3)_4N^+$ (buffer C, △, ▲). These changes result in an increase of the resistance from 36 kΩ cm^2 for buffer A to 53 kΩ cm^2 for buffer B to 250 kΩ cm^2 for buffer C. These results compare favorably to the 46 kΩ cm^2 reported by Purrucker et al. (for 100 mM Na^+) and 680 kΩ cm^2 for $(CH_3)_4N^+$.[38] The decrease in resistance in the presence of $(CH_3)_4N^+$ reported here compared to that reported by Purrucker can be explained by two possible factors: the degradation of the bilayer with time or an incomplete exchange of the K^+ or Na^+ bathing solutions.

Similar results as previously described for melittin can be obtained when observing the in-phase admittance for gramicidin D. Figure 7 (solid line) shows the conductance of gramicidin channels incorporated into a tBLM in the presence of K^+ ions. As the DC potential is scanned from positive to negative potentials, an initial basic conductance is noted at ~4×10^{-5} S/cm^2. At ~0.027 V, a sharp peak (fwhm ≈ 12 mV) ~2.3×10^{-4} S/cm^2 high is observed, followed by a steady-state conductance of 5×10^{-5} S/cm^2. Beyond ~−0.2 V the conductance increases gradually to the reversal potential of −0.5 V. The reverse scan follows the trend in the forward scan from −0.5 to ~0 V. At this point, the reverse scan maintains a conductivity of 5×10^{-5} S/cm^2 until a narrow peak (fwhm ≈ 10 mV) at −0.127

V is observed. Beyond the peak, the conductivity attains the original basic conductance of $\sim 4 \times 10^{-5}$ S/cm^2. The peak separation of ~100 mV is significantly smaller than the observed 130 mV for melittin channels in similar bilayers.

As a control experiment, the buffer cation was switched from K^+ to $(CH_3)_4N^+$ which should be too large to be transported by a gramicidin channel (Figure 7 dashed line). The conductivity is severely diminished as K^+ is excluded from the experiment. This result indicates that all of the observed conductivity with K^+ present can be attributed to K^+ ions specifically transported by the protein rather than nonspecific electric field driven membrane decomposition. The small peak in the reverse wave can be attributed to small amounts of residual K^+ remaining after the exchange of buffers.

Potential dependent ion transport through gramicidin channels incorporated into tBLMs were reported previously.[26] The physical model proposed relied on changes in the potential drop across the membrane as a function of applied potential rather than the details of the transport process. More detailed kinetic analysis of gramicidin-mediated ion transport in solid-supported lipid bilayers can be found in the papers by Steinem et al.[42] and later by Gervasi et al.[43] In these reports, the EIS spectra were analyzed on the basis of equivalent circuits using the continuum model of ion transport according to which diffusion and migration of ions is regarded to take place within the membrane considered to be a thin homogeneous macroscopic phase. Potential dependence was only considered in terms of small ac perturbation on the fitted values for their equivalent circuit (i.e., no potential dependent experiments were performed). In Steinem's treatment, the authors consider the binding and desorption of the cation to the ion channel to be the potential dependent step. Other ion mobility is considered to be simple diffusion and migration. We prefer to attribute the rate-limiting behavior to transport within the channel for the activated process as utilized by Gervasi. In this case, the rate coefficients for the forward and reverse transport, k_f and k_b, are potential dependent according to eq 4 and 5

$$k_f = k_t \exp[F\Delta E/2RT] \quad (4)$$

$$k_b = k_t \exp[-F\Delta E/2RT] \quad (5)$$

where k_t is the potential independent, and thus the directionally independent K^+ transport rate constant and ΔE is the transmembrane potential. When nonpotential dependent K^+ binding and dissociation rate constants at the solution/membrane and membrane/spacer interfaces are included, these relationships suggest a sigmoidal increase in the ion flux and hence a sigmoidal increase in the admittance as the electrode potential is swept negatively.

The sharp peaks noted in these tBLM/protein systems suggest a further limit to the observable admittance in the experiment. Two factors limit the capacity of the submembrane space: the transmembrane charge balance and the physical volume of the spacer. The volume limitation suggests a maximum physical space for cation "storage", whereas the charge balance suggests that the electrical capacitance of the submembrane space will change as ions accumulate.[44]

The potential dependence of the channel activity is further supported by two other observations. First, the peak positions are reproducible within ±5 mV and are different for each channel. Second the specificity of the peak positions as shown by the ~30 mV difference in the peak hysteresis between the gramicidin D and the melittin containing membranes show a striking difference between the two ion channels in similarly constructed membranes demonstrated in Figures 5 and 7. This suggests channel specific rate coefficients of ion transfer k_t. The hysteresis can be accounted for by changes in the electrical potential distribution as ions accumulate in the submembrane space during the forward potential sweep. The accumulation of potassium cations in the submembrane space is expected to cause the applied potential to drop across the oxyethylene spacer rather than the lipid layer. This assertion is deduced from simulations that are currently conducted in our laboratory and which will be published in a forthcoming paper. Upon reversal of the potential sweep direction, the net K^+ flow is from the submembrane space to the bulk solution; however, if much of the potential drop after K^+ accumulation occurs in the submembrane space rather than across the membrane, a more positive potential will be required to expel the ions from the submembrane space.

The increased admittance observed at a potential significantly negative from the peaks arising from carrier transport can be attributed to increased ionic permeability of the tBLM. This permeability effect can be subtly noted in the "blank" sample, which under ideal conditions would show no admittance changes over the entire observed potential range.

For a quantitative treatment of these considerations, detailed modeling studies of the data reported in this paper are currently under way in this laboratory. Such modeling studies using the software package WinSpice have been carried out previously for ion transport through a tBLM mediated by valinomycin.[28]

Conclusions

tBLMs on gold on the basis of mixed SAMs made from the DPTL thiolipid diluted with a complementary hydrophilic thiol spacer unit were designed to allow for incorporation of helical ion channels which were previously shown to fail in undiluted systems. Low fractions of the dilution molecule (20% on the surface according to 10% in solution) are sufficient to allow for the protein incorporation while at the same time preserving the integrity of the bilayer membrane. The conductance was found comparable with that reported for other supported and tethered bilayer systems. Measurements of the in phase component of the admittance at a constant frequency and varying DC potential showed interesting features which were discussed on a qualitative basis in comparison to similar data presented by other groups. Further modeling studies are expected to bring about a more thorough quantitative understanding of the underlying processes.

Acknowledgment. Critical reading of the manuscript and helpful discussions by D. Walz, Biozentrum Basel, are gratefully acknowledged. We also thank Gretl Dworschak, MPI for Polymer Research, for expert technical assistance.

LA051771P

(42) Steinem, C.; Janshoff, A.; Galla, H.-J.; Sieber, M. *Bioelectrochem.* **1997**, *42*, 213.
(43) Vallejo, A. E.; Gervasi, C. A. *Bioelectrochem.* **2002**, *57*, 1.
(44) Krishna, G.; Schulte, J.; Cornell, B. A.; Pace, R.; Wieczorek, L.; Osman, P. D. *Langmuir* **2001**, *17*, 4858.